European Journal of Chemistry

Check for updates

View Journal Online
View Article Online

Synthesis, crystal structure, and Hirshfeld surface analysis of a cubane-type tetranuclear polyoxotitanate cluster

Jayanta Kumar Nath

Department of Chemistry, Sreenivas Basudev Deorah College, Ulubari, Guwahati, Assam-781007, India

** Corresponding author at: Department of Chemistry, Sreenivas Basudev Deorah College, Ulubari, Guwahati, Assam-781007, India.*
e-mail: jay123.nath@gmail.com (J.K. Nath).

RESEARCH ARTICLE

10.5155/eurjchem.16.2.146-153.2646

Received: 16 January 2025
Received in revised form: 6 March 2025
Accepted: 20 April 2025
Published online: 30 June 2025
Printed: 30 June 2025

KEYWORDS

Cubane
Carboxylic acids
Naphthalic anhydride
Polyoxotitanate cluster
Hirshfeld surface analysis
Supramolecular chemistry

ABSTRACT

A cubane-type tetranuclear polyoxotitanate cluster derived from 8-(isopropoxycarbonyl)-1-naphthoic acid is reported which is synthesized under reflux conditions in isopropanol (HO^iPr). The ligand 8-(isopropoxycarbonyl)-1-naphthoic acid (INA) was generated *in situ* from 1,8-naphthalic anhydride and isopropyl alcohol in the reaction mixture where one of the carboxylate groups of 1,8-naphthalene dicarboxylic acid (generated from the ring opening reaction of 1,8-naphthalic anhydride) forms isopropyl ester by reacting with solvent isopropoxide. The solid-state structural elucidation of the cluster is achieved through the single crystal X-ray diffraction method, providing detailed insights into their molecular arrangements. Crystal data for $C_{72}H_{80}O_{24}Ti_4$: Triclinic, space group *P*-1 (no. 2), a = 19.086(3) Å, b = 20.341(4) Å, c = 21.538(4) Å, α = 88.895(4)°, β = 72.158(4)°, γ = 89.049(4)°, V = 7958(3) Å^3, Z = 4, T = 293(2) K, μ(MoKα) = 0.457 mm^{-1}, *Dcalc* = 1.269 g/cm^3, 64356 reflections measured (4.42° ≤ 2Θ ≤ 54.94°), 34455 unique (R_{int} = 0.0458, R_{sigma} = 0.0752) which were used in all calculations. The final R_1 was 0.0603 (>2sigma(I)) and wR_2 was 0.1558 (all data). In the crystal lattice, the asymmetric unit of the cluster contains two molecules. Various types of supramolecular interactions such as C-H···O, C-H···π, π···π and unusual O···O interactions are observed in the X-ray structures. All these interactions guide the formation of 3D supramolecular architecture in the solid state of the compound. In addition to these, 2D fingerprint (2D-FP) and Hirshfeld surface analysis (HSA) computations were used to prove and quantify various supramolecular interactions within the crystal lattice.

Cite this: *Eur. J. Chem.* **2025**, *16(2)*, 146-153 **Journal website**: www.eurjchem.com

1. Introduction

Titanium oxo clusters are intriguing molecules that often display properties comparable to those of bulk or nano-TiO_2 materials [1,2]. Titanium oxo clusters can be used in bulk materials, as catalytic sites, and in dye-sensitized materials [3-5]. The advantage of these compounds lies in their ability to tailor their physicochemical, photocatalytic, and biological properties by modifying the core size and architecture of $\{Ti_aO_b\}$ and functionalizing carboxylate groups as stabilizing ligands [6-9], *etc*. Furthermore, TiO_2 finds applications in photocatalysis, solar cells, and remediation of environmental pollution [10-16]. Polyoxotitanate clusters (POT) or titanium oxo clusters (TOCs) with well-defined structures are considered ideal molecular models for TiO_2 materials [17,18]. As POTs are protected by ligands, they can provide information about the relationship between the structure and properties of TiO_2 and surface structural information [9,19,20]. Furthermore, transition-metal-based carboxylate complexes [21-25], especially POT, show various supramolecular interactions and assemblies [26]. Naphthalene and its derivatives have been widely studied for their attractive photophysical properties, primarily because of excimer formation. The UV-visible spectra of 2- or 3-ring Poly Aromatic Hydrocarbons (PAHs), such as naphthalene, exhibit strong ultraviolet absorption from π-π* transitions and a distinct fine structure linked to conjugated aromatic bonds [27,28]. This adds additional properties to the cluster as a photocatalyst. Although there are several reports on polyoxotitanate clusters based on carboxylate ligands, POT formed from 1,8-naphthalene dicarboxylic acid or its derivatives is very rare.

Keeping this in mind here, we report crystal structure of a tetranuclear cubane-type polyoxotitanate cluster of $[Ti_4(\mu_3\text{-}O)_4(\mu_2\text{-}INA)_4(O^iPr)_4]$ {O^iPr-: isopropyl alcoholate ion, INA which is formed by the reaction of 1,8-naphthalene dicarboxylic acid (formed ring opening reaction of 1,8-naphthlic anhydride) with solvent (Figure 1) and the core of the cluster consists of Ti_4.

2. Experimental

2.1. Chemicals and reagents

All chemicals, reagents, and solvents were purchased from Sigma-Aldrich or Alfa-Aesar and used as received unless otherwise stated.

2.2. Synthesis of the Ti-cluster

The cluster was synthesized using a solvothermal method in which titanium isopropoxide (1 mmol, 0.298 mL) was added

https://dx.doi.org/10.5155/eurjchem.16.2.146-153.2646

Table 1. Crystallographic parameters of the cluster.

Compound	Ti4-cluster
Empirical formula	$C_{72}H_{80}O_{24}Ti_4$
CCDC deposition number	2405481
formula weight	1610.85
Temperature/K	293(2)
crystal system	Triclinic
space group	*P-1*
a/Å	19.086(3)
b/Å	20.341(4)
c/Å	21.538(4)
α/°	88.895(4)
β/°	72.158(4)
γ/°	89.049(4)
V/Å^3	7958(3)
Z	4
Density (g cm^{-3})	1.269
μ/mm^{-1}	0.457
F(000)	3168.0
Crystal size/mm^3	0.19 × 0.17 × 0.15
Rradiation type	MoKα (λ = 0.71073)
2Θ range for data collection/°	4.42 to 54.94
Index Ranges	$-24 \le h \le 24$, $-26 \le k \le 26$, $-27 \le l \le 27$
Reflections collected	64356
Independent reflections	34455 [R_{int} = 0.0458, R_{sigma} = 0.0752]
Data/Restraints/Parameters	34455/0/ 1833
Goodness-of-fit on F^2	1.047
Final R indexes [I>=2σ (I)]	R_1 = 0.0603, wR_2 = 0.1382
Final R indexes [all data]	R_1 = 0.0922, wR_2 = 0.1558
Largest diff. peak/hole / e Å^{-3}	0.45/-0.39
CCDC deposition number	2405481

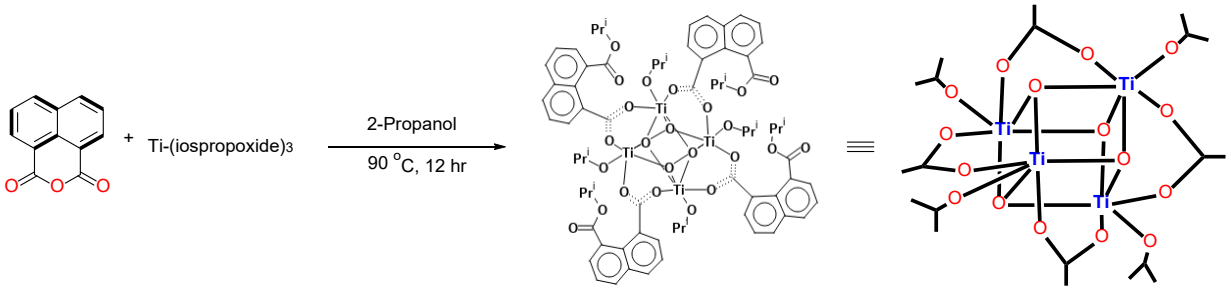

Figure 1. Synthesis of the Ti cluster.

to a solution of 1,8-naphthalic anhydride (1 mmol, 0.298 g) in 2-propanol and the mixture was heated at 90 °C for 24 hr. After being cooled to room temperature, colorless prismatic type crystals were obtained. Yield 78%.

2.3. X-ray crystallography

The cluster crystal that has approximate dimensions of 0.19 mm × 0.17 mm × 0.15 mm was sealed in a glass capillary. Crystallographic data and structure refinement parameters for the cluster at 293(2) K are given in Table 1. X-ray diffraction data were collected on a Rigaku Inc., 2008 Bruker SMART Apex II CCD diffractometer using Mo Kα (λ = 0.71073 Å) radiation and X-ray diffraction data for the crystal were collected using Bruker SMART software [29]. This software was also used for indexing and determination of the unit cell parameters. Cell structures were solved by direct method and refined using full matrix least squares against F^2 of all data, using SHELXTL [30] and Olex2-1.5 [31] software. All non-H atoms were refined by full-matrix least squares in anisotropic symmetry, while all H atoms were refined in an isotropic approximation, against F^2 of all reflections. Some hydrogen atoms attached to these atoms were treated as 'riding' in calculated positions. As the disordered solvent molecules could not be assigned, a Platon-PWT 2023.1 [32] squeeze method is applied to remove the electron density. From the squeeze result, it is observed that a total of 36 electron counts was removed, which is equal to one and half of isopropanol molecules (24 electrons + 12 electrons = 36 electrons). The molecular structures were drawn at Mercury 4.2.0 [33], Diamond software version 3.2 [34]. The selected bond distances (Å) and angles (°) of the Ti-cluster are given in Table 2.

3. Results and discussion

3.1. Crystal structure

The structure of the cluster has been established by single crystal X-ray analysis having composition $[Ti_4(INA)_4(\mu_3\text{-}O)_4(O^iPr)_4]\cdot 1.5C_3H_8O$ and crystallized in the *P*-1 triclinic space group. The asymmetric unit of the cluster contains two molecules of the clusters where each cluster contains four Ti(IV) ions, four coordinated μ_3-INA ligands, four coordinated isopropoxide ions with 3 bridges, four μ_3-bridged oxide ions (Figure 2a). In addition to these, isopropanol molecules of crystallization are also present in its asymmetric unit. The coordination polyhedra around the metal center of the cluster are shown in Figure 2c. The $\{Ti_4(\mu_3\text{-}O_4)\}$ core forms a tetragonally distorted cube with alternately arranged Ti and O atoms organized into Ti_2O_2 faces, linked by four carboxylate groups. The Ti ions form a cubane type structure with the oxide ions, as shown in Figure 2b. The Ti···Ti distance in the cubane-type structure is in the range of 2.9167(8)-3.045(8) Å. Each Ti^{4+} ion in the cluster is in a $\{TiO_6\}$ environment and adopted a distorted octahedra coordination geometry around the metal center.

Table 2. Selected bond distances (Å) and angles (°) of the Ti-cluster.

M-L	d_{M-L}(Å)	∠L-M-L	Angle (°)	∠L-M-L	Angle (°)	∠L-M-L	Angle (°)
Ti1-024	3.045(8)	O24-Ti1-O26	63.2(3)	O30-Ti4-019	162.75(8)	O14-Ti7-02	91.55(8)
TI1-026	2.0576(7)	O24-Ti1-O32	82.42(8)	O30-Ti4-021	88.27(7)	O14-Ti7-05	161.50(8)
Ti1-029	1.8958(18)	O26-Ti1-O32	110.9(2)	O30-Ti4-031	81.67(7)	O14-Ti7-012	81.36(7)
Ti1-031	1.9509(18)	O29-Ti1-O24	90.69(8)	O31-Ti4-021	82.95(7)	O14-Ti7-013	80.08(8)
Ti1-032	2.1082(18)	O29-Ti1-O26	161.71(8)	O32-Ti4-019	90.34(8)	O18-Ti7-02	98.47(10)
Ti1-048	1.745(2)	O29-Ti1-O31	80.44(7)	O32-Ti4-021	163.33(8)	O18-Ti7-05	92.76(9)
Ti2-022	2.0408(19)	O29-Ti1-O32	81.70(7)	O32-Ti4-030	81.34(8)	O18-Ti7-012	174.72(9)
Ti2-023	2.0313(19)	O31-Ti1-O24	161.89(8)	O32-Ti4-031	82.66(7)	O18-Ti7-013	99.09(9)
Ti2-029	2.1079(17)	O31-Ti1-O26	87.29(8)	O46-Ti4-019	94.43(9)	O18-Ti7-014	103.83(9)
Ti2-030	1.9224(17)	O31-Ti1-O32	80.70(7)	O46-Ti4-021	90.43(9)	O3-Ti8-06	96.41(8)
Ti2-032	1.9457(19)	O48-Ti1-O24	133.3(3)	O46-Ti4-030	102.26(9)	O3-Ti8-014	81.66(7)
Ti2-039	1.7510(19)	O48-Ti1-O26	91.88(9)	O46-Ti4-031	172.23(8)	O6-Ti8-014	82.55(8)
Ti3-020	2.0774(19)	O48-Ti1-O29	104.03(9)	O46-Ti4-032	104.46(9)	O11-Ti8-03	90.61(8)
Ti3-025	2.0556(19)	O48-Ti1-O31	103.15(9)	O8-Ti5-O7	96.41(8)	O11-Ti8-06	162.17(8)
Ti3-029	1.9239(18)	O48-Ti1-O32	173.48(9)	O8-Ti5-O11	82.20(8)	O11-Ti8-012	81.12(8)
Ti3-030	2.0838(17)	O22-Ti2-O29	82.08(7)	O11-Ti5-O7	162.70(8)	O11-Ti8-014	82.28(7)
Ti3-031	1.9111(18)	O23-Ti2-O22	94.89(8)	O13-Ti5-O8	91.24(8)	O12-Ti8-03	162.51(8)
Ti3-047	1.7622(19)	O23-Ti2-O29	82.34(7)	O13-Ti5-O11	82.66(7)	O12-Ti8-06	87.53(8)
Ti4-019	2.057(2)	O30-Ti2-O22	161.04(8)	O13-Ti5-O14	80.85(8)	O12-Ti8-014	81.97(7)
Ti4-021	2.0903(18)	O30-Ti2-O23	91.47(8)	O14-Ti5-O7	87.44(8)	O16-Ti8-03	94.40(8)
Ti4-030	1.9261(18)	O30-Ti2-O29	81.09(7)	O14-Ti5-O8	162.59(8)	O16-Ti8-06	89.02(9)
Ti4-031	2.0818(18)	O30-Ti2-O32	80.18(7)	O14-Ti5-O11	81.43(7)	O16-Ti8-011	106.82(9)
Ti4-032	1.8963(18)	O32-Ti2-O22	88.51(8)	O17-Ti5-O7	89.25(8)	O16-Ti8-012	102.72(8)
Ti4-046	1.7656(19)	O32-Ti2-O23	161.95(8)	O17-Ti5-O8	95.75(9)	O16-Ti8-014	170.21(9)
Ti5-O7	2.0960(19)	O32-Ti2-O29	80.57(7)	O17-Ti5-O11	171.74(8)		
Ti5-O8	2.054(2)	O39-Ti2-O22	92.55(9)	O17-Ti5-O13	105.43(9)		
Ti5-O11	2.0848(17)	O39-Ti2-O23	95.19(9)	O17-Ti5-O14	101.29(9)		
Ti5-O13	1.8929(18)	O39-Ti2-O29	173.85(8)	O1-Ti6-O13	81.91(8)		
Ti5-O14	1.9380(19)	O39-Ti2-O30	104.66(9)	O4-Ti6-O1	96.36(9)		
Ti5-O17	1.7679(19)	O39-Ti2-O32	102.38(9)	O4-Ti6-O13	82.15(8)		
Ti6-O1	2.551(7)	O20-Ti3-O30	83.76(7)	O11-Ti6-O1	88.18(8)		
Ti6-O4	2.024(2)	O25-Ti3-O20	99.17(8)	O11-Ti6-O4	161.39(8)		
Ti6-O11	1.9558(18)	O25-Ti3-O30	81.95(7)	O11-Ti6-O13	80.64(7)		
Ti6-O12	1.9042(19)	O29-Ti3-O20	86.58(8)	O12-Ti6-O1	161.47(8)		
Ti6-O13	2.1063(18)	O29-Ti3-O25	161.94(8)	O12-Ti6-O4	90.30(9)		
Ti6-O15	1.7564(19)	O29-Ti3-O30	81.68(7)	O12-Ti6-O13	81.91(8)		
Ti7-02	2.024(2)	O31-Ti3-O20	162.11(8)	O15-Ti6-O1	92.30(9)		
Ti7-05	2.065(2)	O31-Ti3-O25	89.46(8)	O15-Ti6-O4	98.40(9)		
Ti7-012	2.1150(18)	O31-Ti3-O29	80.75(7)	O15-Ti6-O11	99.44(8)		
Ti7-013	1.9465(19)	O31-Ti3-O30	81.97(7)	O15-Ti6-O12	103.83(9)		
Ti7-014	1.9152(18)	O47-Ti3-O20	89.97(9)	O15-Ti6-O13	174.21(9)		
Ti7-018	1.757(2)	O47-Ti3-O25	94.08(9)	O2-Ti7-O5	94.09(9)		
Ti8-O3	2.0503(19)	O47-Ti3-O29	103.08(9)	O2-Ti7-O12	82.20(8)		
Ti8-O6	2.062(2)	O47-Ti3-O30	171.92(9)	O5-Ti7-O12	81.97(8)		
Ti8-O11	1.9042(19)	O47-Ti3-O31	105.11(9)	O13-Ti7-O2	161.92(8)		
Ti8-O12	1.9252(18)	O19-Ti4-O21	96.04(8)	O13-Ti7-O5	89.37(9)		
Ti8-O14	2.0828(18)	O19-Ti4-O31	82.29(7)	O13-Ti7-O12	80.72(7)		

Table 3. Some of the hydrogen bond parameters such as C-H···O, and C-H···π, π···π contacts for the cluster.

Donor-H···Acceptor	D···A (Å)	D-H···A (Å)	Angle A···H···A (°)
C104-H10A···O41	2.53	3.055(5)	115
C104-H10C···O29	2.39	3.312(4)	160
C111-H11A···O36	2.46	3.038(6)	118
C117-H11S···O10	2.48	3.035(5)	117
C121-H12C···O34	2.58	3.103(7)	114
C133-H13I···O45	2.48	3.045(8)	117
C139-H13P···O42	2.42	2.992(8)	118
C146-H14R···O38	2.53	3.035(8)	113
C19-H19···O45	2.38	3.045(8)	164
C28-H28···O2	2.43	2.756(5)	101
C28-H28···O42	2.32	3.148(6)	148
C30-H30···O8	2.47	2.789(5)	100
C30-H30···O10	2.35	3.257(5)	164
C36-H36···O4	2.47	2.787(4)	100
C36-H36···O38	2.28	3.140(6)	155
C54-H54···O25	2.43	2.757(4)	101
C54-H54···O36	2.33	3.241(4)	167
C59-H59···O23	2.42	2.749(4)	100
C59-H59···O41	2.57	3.312(5)	137
C73-H73···O19	2.43	2.759(4)	100
C73-H73···O34	2.28	3.176(5)	161
C77-H77···O28	2.46	2.823(5)	100
C86-H86···O24	2.46	2.775(4)	100
C86-H86···O28	2.31	3.184(5)	156
C88-H88···O9	2.49	3.407(5)	167
C94-H94···O41	2.46	2.788(5)	100
C12- H12···O36	2.67	3.501(4)	148.71
C123-H12I···O15	2.69	3.650 (5)	174.11
C64-H64···O10	2.66	3.373(5)	133.50

Table 3. (Continued).

C-H···Cg	C···Cg (Å)
C137-H13E···Cg	3.766
C111-H11B···Cg	3.797
C89-H89··· Cg	3.924
Cg···Cg	3.587

Cg = Center of gravity of the ring.

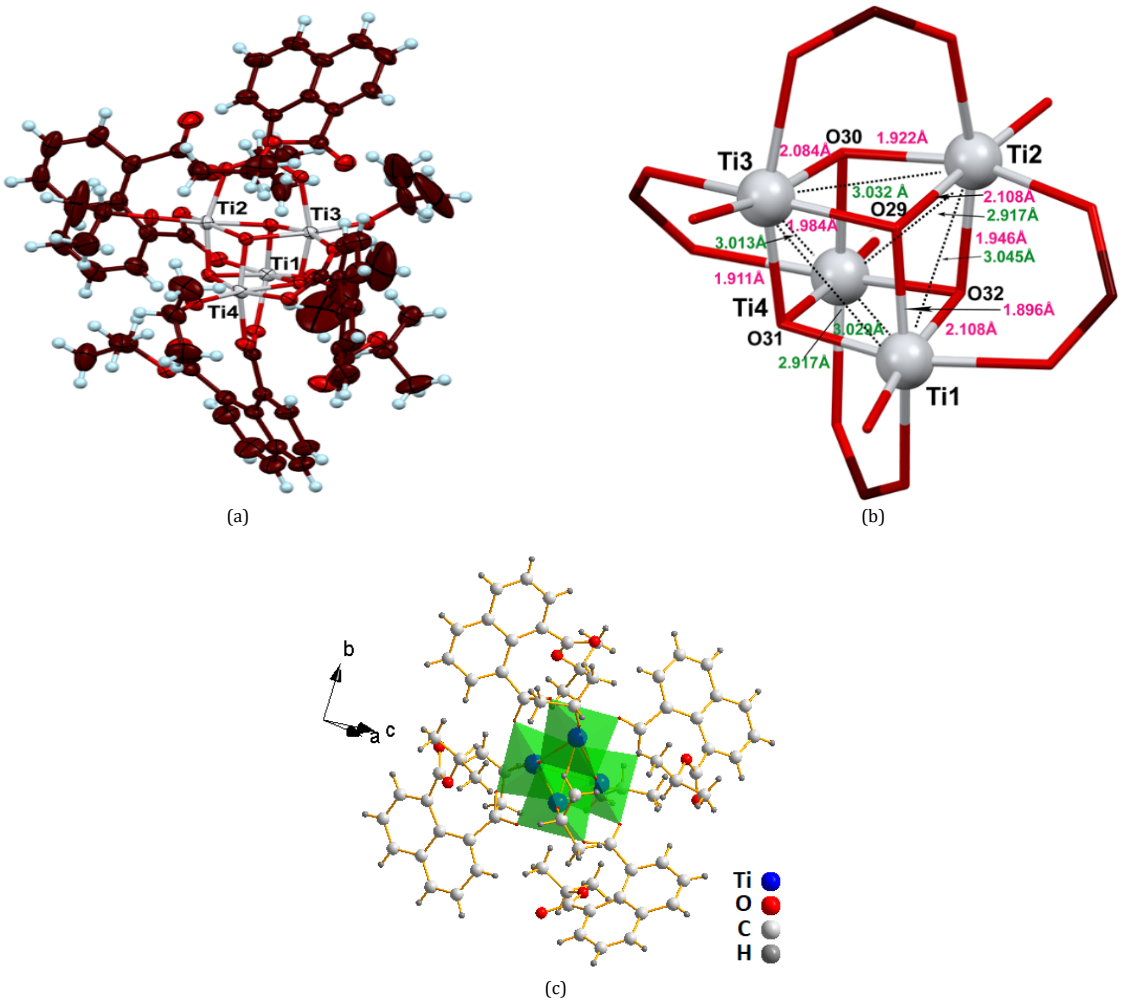

Figure 2. (a) Ellipsoid view (40% thermal ellipsoid) of the cluster, (b) Different coordination environment around Ti center, (c) Coordination polyhedra around Ti.

The octahedral geometry is satisfied by two O atoms from two carboxylate groups of two different ligands and three O atoms from three oxide ligands, as shown in Figure 2b. Each carboxylate group of the ligand acts as a bridging ligand between two Ti^{4+} ions in which Ti binds with O with unequal bond length ranging from 2.024-2.090 Å. Polyhedral structure of the cluster around the Ti center has been shown in the Figure 4a. These bonds are little shorter than some reported transition metal-carboxylate bond [21]. The core structure is a distorted cubane-type structure which is reflected from the unequal Ti-oxo bond length ranging from d_{Ti-O} = 1.896-2.108 Å and from the Ti-O-Ti bond angle ∠Ti-O-Ti which vary from 97.3 to 98.9° whereas ∠O-Ti-O bond angles vary from 80.70° to 82.67°. The Ti-Ti distances corresponding to the diagonal of rectangular Ti_2O_2 faces are close to 2.917 Å, while Ti–Ti distances between atoms belonging to different faces are close to 3.045 Å. The four terminal Ti-O bond lengths of coordinated isopropoxide ions are different and shortest which vary from 1.745 Å to 1.766 Å in one unit, whereas in the other unit this distance varies from 1.756 to 1.775 Å. The detailed metal ligand bond parameters are shown in Table 2. These parameters are comparable to the reported Ti clusters [35]. There are several supramolecular (intermolecular) interactions that exist in the solid-state structure of the cluster, such as C-H···O and C-H···π (both aromatic and aliphatic C-H) interactions. The weak donor-acceptor distance of these C-H···O hydrogen bonds are C64-H64···O10 ($d_{C64-O10}$ = 3.373 (5) Å), C12-H12···O36 bond ($d_{C12-O36}$ = 3.501(4) Å), C123-H12I···O15 ($d_{C123-O15}$ = 3.650 (5) Å) and C88-H88···O9 (d_{C88-O9} = 3.407(5) Å) (Figure 3a,b). The bond angle of these hydrogen bonds are <C12-H12-O36 = 148.71°, <C123-H12I-O15 = 174.11°, C64-H64···O10 = 133.50° and <C88-H88-O9 = 167°. The H bonding table is shown in Table 3.

An unusual intramolecular O···O interaction is observed with distance ranging from 2.831 to 2.911 Å in one unit and this distance in the other unit vary from 2.898 to 3.019 Å. In addition to these H bonds, the crystal structure is further stabilized by C-H···π with $d_{C\cdots Cg}$ (Cg means center of gravity of the ring) ranging from 3.766 to 4.221 Å and π···π interaction with $d_{Cg\cdots Cg}$ distance of 3.857 Å which has been shown in Figure 4b. All these interactions lead to the formation of a 3D supramolecular structure in the solid state (Figure 3c), and the 3D architecture space fill model is also shown in Figure 3d.

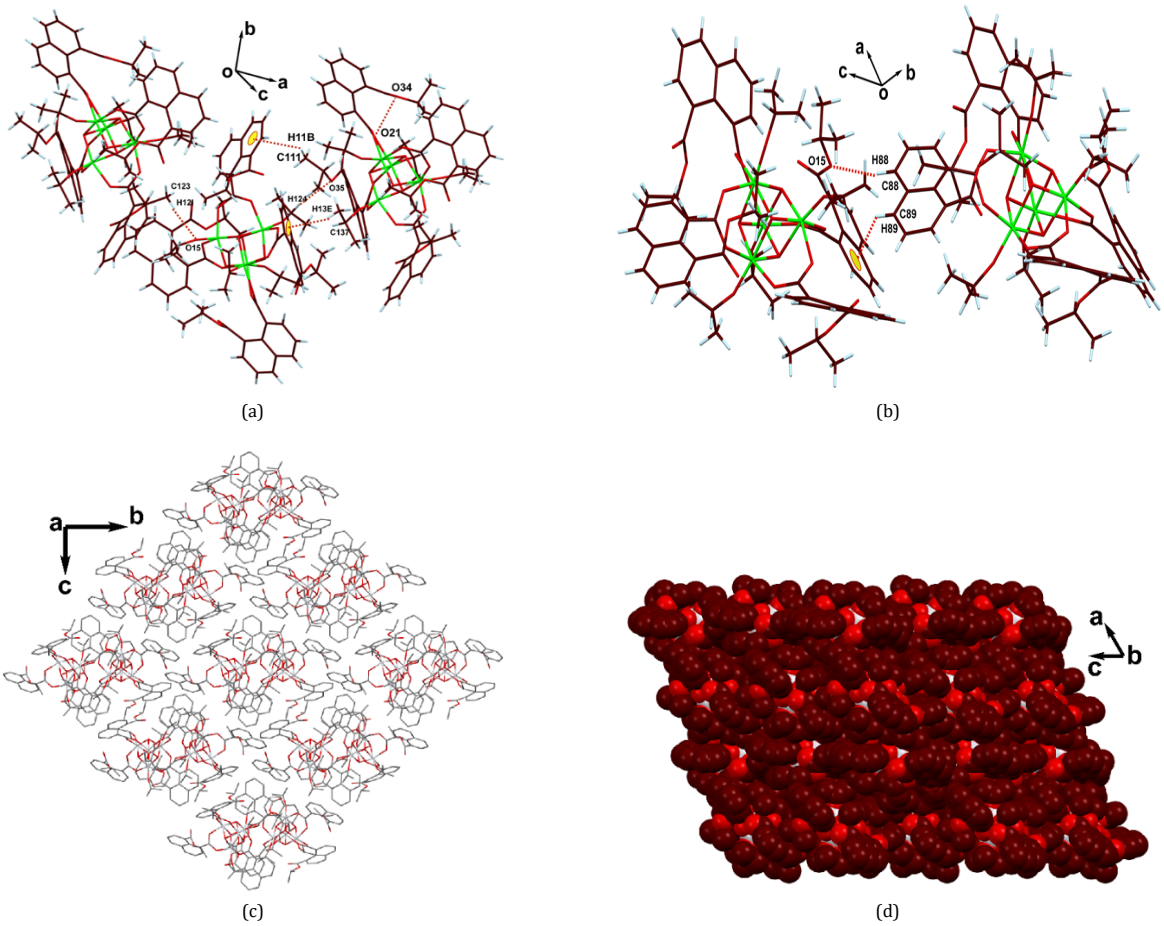

(a) (b)

(c) (d)

Figure 3. (a) Aliphatic C-H···π, C-H···O and O···O interactions, (b) Aromatic C-H···O, C-H···π interactions, (c) 3D supramolecular structure, and (d) packing diagram (space fill model).

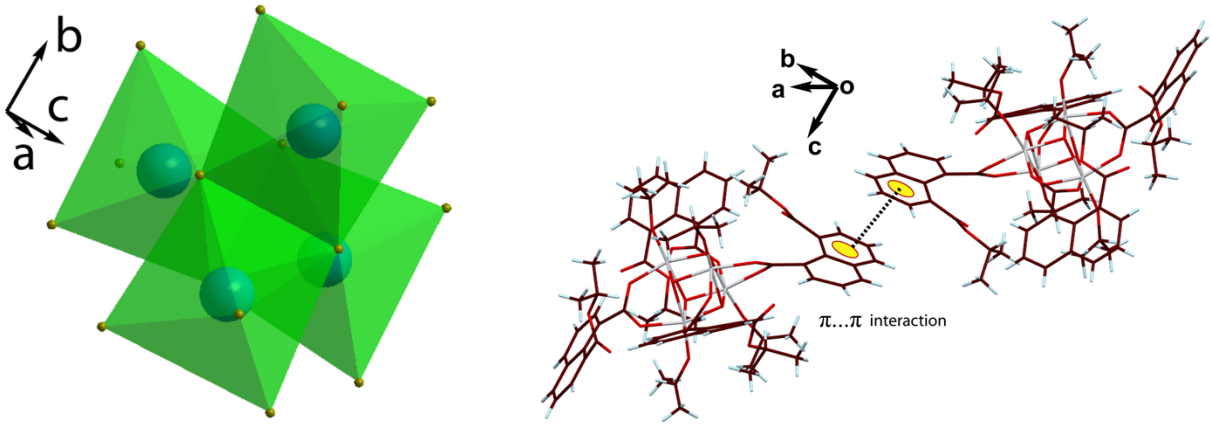

(a) (b)

Figure 4. (a) Polyhedral structure of the cluster around the Ti center and (b) π···π interaction in the cluster.

3.2. Hirshfeld surface and 2-dimensional fingerprint plot analysis

Hirshfeld surface analysis was performed and associated two-dimensional fingerprint plots were generated using CrystalExplorer 21 [36], with a standard resolution of the three-dimensional d_{norm} surfaces plotted over a fixed color scale of -0.1614 to 6.8691 a.u. Figure 5 highlights various contacts on the molecular Hirshfeld surface, mapped using standard indices such as d_{norm}, d_e, shape index, curvedness, and fragment patches. The different colors of the Hirshfeld surface mapped over d_{norm} relate to different distances. A red surface indicates distances shorter than the sum of van der Waals radii (close and strong intermolecular interactions such as C-H···O), a white surface indicates distances near the sum of van der Waals radii (it represents neutral areas where weak van der Waals interactions), and a blue surface indicates distances longer than the sum of van der Waals radii (it corresponds to areas of positive electrostatic potential, meaning they are electron deficient).

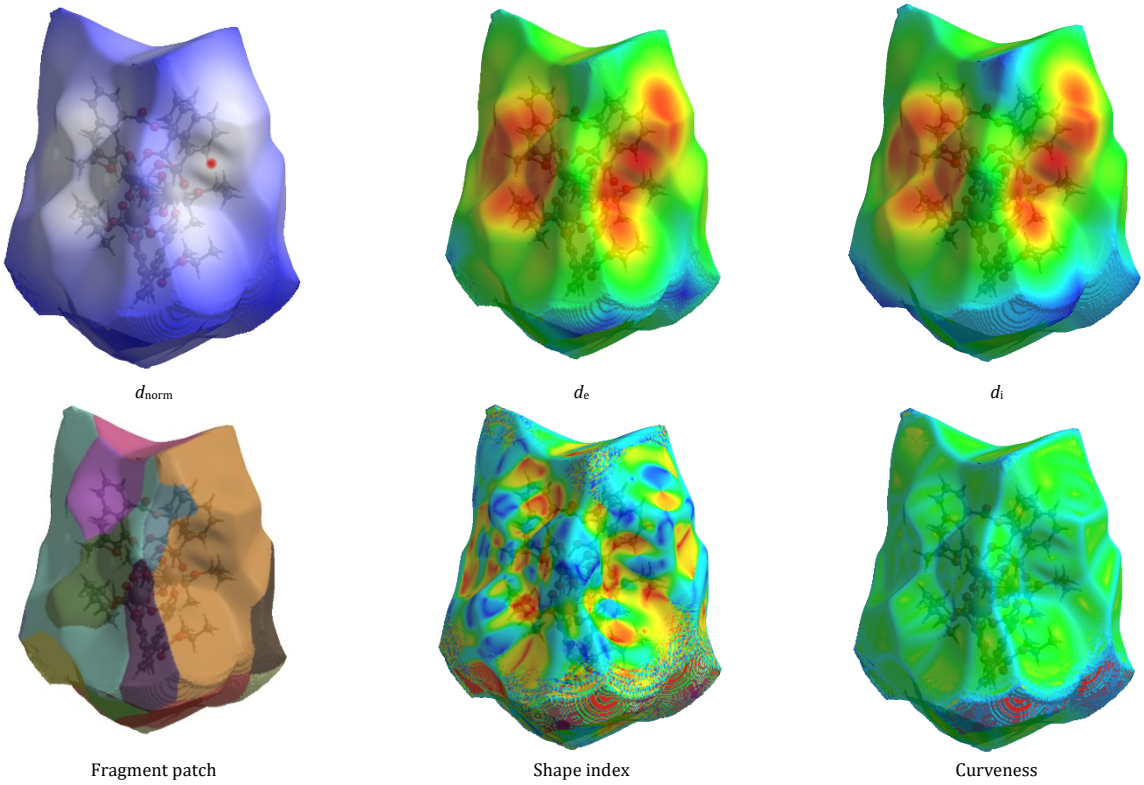

Figure 5. Three-dimensional Hirshfeld surfaces mapped with d_{norm}, d_e, shape-index surfaces showing π···π interactions, with red and blue triangles within a black ellipse indicating bumps and hollow regions, respectively, evidencing the π···π stacking area on the Hirshfeld surfaces, curvedness with flat areas emphasizing the ring contributions in π-stacking interactions and fragment patches showing different colors of fragment patches represent molecular interactions across the molecular region of the compounds of Ti-cluster.

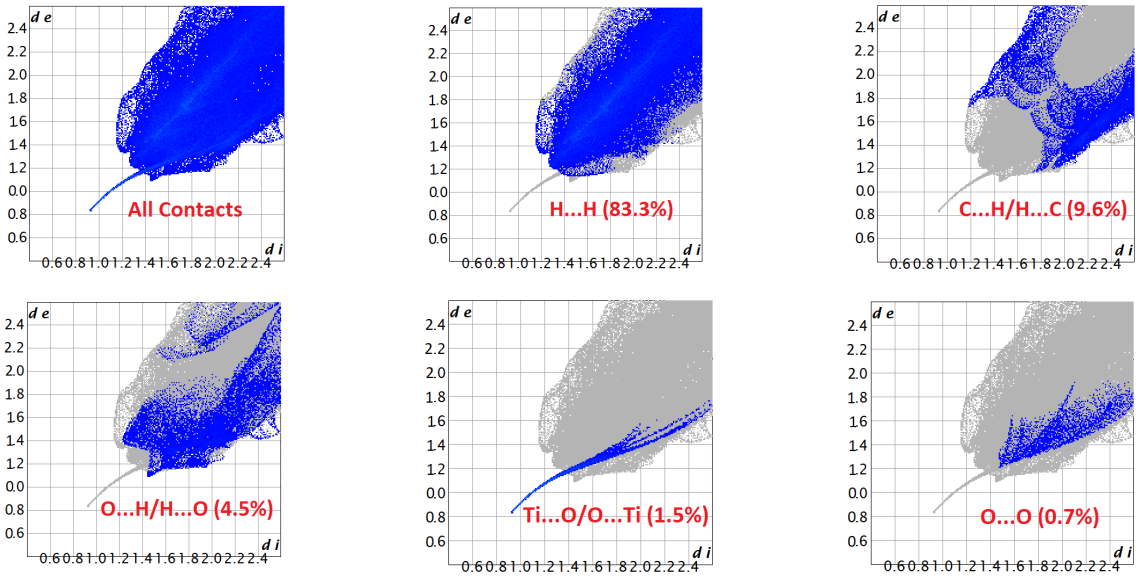

Figure 6. The full 2D-FP for the Ti cluster showing all interactions and delineated into H···H, C···H/H···C, O···H/H···O, Ti···O/O···Ti and C···C, interactions. The d_i and d_e values are the closest internal and external distances (in Å) from given points on the HS contacts.

Certain areas on the d_{norm} surfaces represent H···H close contacts and non-classical hydrogen bond interactions. The surface of the shape index surface shows complementary triangular pairs upon 180° rotation, a key feature of π···π stacking essential for the molecular stability and self-assembly of aromatic compounds [37,38]. The red and blue triangles within a black ellipse indicate bumps and hollow regions, respectively, evidencing the π···π stacking area on the Hirshfeld surfaces. Curvedness surfaces of the cluster further confirm π···π interactions, with flat areas indicating a close proximity of the aromatic ring. These interactions significantly impact molecular conformation and reactivity. Different colors of fragment patches represent molecular interactions across the molecular region. The volume within the Hirshfeld surface is computed to be 3438.74 Å^3, with an area of 1677.09 Å^2.

This analysis provides more information about the intermolecular interactions within the crystal lattice of the cluster. The main objective of this study was to quantitatively analyze the various intermolecular interactions, shedding light on the subtle contacts that intricately shape the molecule. Notably, the light red spots on the HS predominantly correspond to significant types of intermolecular interactions: C-H···O, C-H···π and π···π.

Directional dihydrogen intramolecular interactions, such as C-H···H-C, have been observed in the crystal structure, as illustrated in Figure 5. These interactions were theoretically reported by Almeida *et al.* [39], demonstrating that dihydrogen contacts are sufficiently strong and directional to stabilize molecular arrangements in crystals [40]. Additionally, theoretical studies have explored the behavior of dihydrogen contacts in greater detail [41,42]. All these interactions contribute to the stability of a compound in the solid state [43]. In our cluster, the H···H interaction is found to be the most prominent interaction, which contributes 83.3% of the overall interaction strength. These provide stability to the overall crystal packing which is due to a large number of the short interatomic H···H contacts that are located in the middle region of the fingerprint plot reflected in the plot [44,45]. This indicates that weak van der Waals forces significantly contribute to the compound's cohesive nature. [46]

The other contributions such as C···H/H···C, O···H/H···O, O···O and C···C contacts are 9.6, 4.5, 0.7 and 0.4%, respectively (Figure 6). An unusual Ti···O/O···Ti interaction is observed which contributes 1.5% to the overall crystal packing [47]. The C···C interaction signifies the π···π stacking interaction in the solid-state structure. and this interaction is essential for the molecular stability and self-assembly of aromatic compounds [48-51].

4. Conclusions

In conclusion, a tetranuclear polyoxotitanate cluster exhibiting a cubane-type structure based on a naphthalene carboxylate mono ester-based ligand was successfully synthesized and subsequently characterized with SCXRD. The solid-state X-ray crystal structure of the cluster forms 3D supramolecular structures, driven by noncovalent interactions like C–H···O, C–H···π, and π···π interactions. The primary contributor to the solid-state structures was identified through the 2D fingerprint plot in Hirshfeld surface analysis. Among all interactions, dihydrogen interactions contribute the most, playing a crucial role in stabilizing the overall packing of the solid-state structure. Because of the presence of naphthalene rings in the cluster, this material could provide an arena for researchers to delve into a novel direction in the advancement of the photocatalyst molecule and provides insights into structural diversity and supramolecular phenomena.

Acknowledgements

The author thanks ANRF (SERB-TARE) for research grant with file no. TAR/2023/000221. The author acknowledges Sreenivas Basudev Deorah College for laboratory facility and the Indian Institute of Technology Guwahati for single crystal X-ray Diffraction facility.

Supporting information

CCDC-2405481 contains the supplementary crystallographic data for this paper. These data can be obtained free of charge via www.ccdc.cam.ac.uk/data request/cif, or by e-mailing data request@ccdc.cam.ac.uk, or by contacting The Cambridge Crystallographic Data Centre, 12 Union Road, Cambridge CB2 1EZ, UK; fax: +44(0)1223-336033.

Disclosure statement

Conflict of interest: The authors declare that they have no conflict of interest.
Ethical approval: All ethical guidelines have been adhered.
Sample availability: Samples of the compounds are available from the author.

ORCID and Email

Jayanta Kumar Nath
jay123.nath@gmail.com
https://orcid.org/0000-0002-0477-5861

References

[1]. Schubert, U. Titanium-Oxo Clusters with Bi- and Tridentate Organic Ligands: Gradual Evolution of the Structures from Small to Big. *Chemistry A. European J.* **2021**, *27* (44), 11239–11256.
[2]. Fang, W.; Zhang, L.; Zhang, J. Synthetic strategies, diverse structures and tuneable properties of polyoxo-titanium clusters. *Chem. Soc. Rev.* **2018**, *47* (2), 404–421.
[3]. Zhu, Q.; Dai, J. Titanium oxo/alkoxyl clusters anchored with photoactive ligands. *Coord. Chem. Rev.* **2021**, *430*, 213664.
[4]. Fan, Y.; Cui, Y.; Zou, G.; Duan, R.; Zhang, X.; Dong, Y.; Lv, H.; Cao, J.; Jing, Q. A ferrocenecarboxylate-functionalized titanium-oxo-cluster: the ferrocene wheel as a sensitizer for photocurrent response. *Dalton Trans.* **2017**, *46* (25), 8057–8064.
[5]. Fan, X.; Wang, J.; Wu, K.; Zhang, L.; Zhang, J. Isomerism in Titanium-Oxo Clusters: Molecular Anatase Model with Atomic Structure and Improved Photocatalytic Activity. *Angew Chem Int Ed* **2018**, *58* (5), 1320–1323.
[6]. Piszczek, P.; Radtke, A.; Muzioł, T.; Richert, M.; Chojnacki, J. The conversion of multinuclear μ-oxo titanium(iv) species in the reaction of Ti(OiBu)4 with branched organic acids; results of structural and spectroscopic studies. *Dalton Trans.* **2012**, *41* (27), 8261.
[7]. Kubiak, B.; Muzioł, T.; Wrzeszcz, G.; Radtke, A.; Golińska, P.; Jędrzejewski, T.; Wrotek, S.; Piszczek, P. Structural characterization and bioactivity of a titanium(IV)-oxo complex stabilized by mandelate ligands. *Molecules* **2024**, 29(8), 1736, https://doi.org/10.3390/molecules29081736.
[8]. Papiernik, R.; Hubert-Pfalzgraf, L. G.; Vaissermann, J.; Goncalves, M. C. Synthesis and characterization of new titanium hexanuclear oxo carboxylato alkoxides. Molecular structure of [Ti6(μ3-O)6(μ-O2CC6H4OPh)6(OEt)6]. *J. Chem. Soc., Dalton Trans.* **1998**, 2285–2288.
[9]. Lv, H.; Li, H.; Zou, G.; Cui, Y.; Huang, Y.; Fan, Y. Titanium-oxo clusters functionalized with catecholate-type ligands: modulating the optical properties through charge-transfer transitions. *Dalton Trans.* **2018**, *47* (24), 8158–8163.
[10]. Ge, M.; Cao, C.; Huang, J.; Li, S.; Chen, Z.; Zhang, K.; Al-Deyab, S. S.; Lai, Y. A review of one-dimensional TiO_2nanostructured materials for environmental and energy applications. *J. Mater. Chem. A.* **2016**, *4* (18), 6772–6801.
[11]. Bai, Y.; Mora-Seró, I.; De Angelis, F.; Bisquert, J.; Wang, P. Titanium Dioxide Nanomaterials for Photovoltaic Applications. *Chem. Rev.* **2014**, *114* (19), 10095–10130.
[12]. Fujishima, A.; Honda, K. Electrochemical Photolysis of Water at a Semiconductor Electrode. *Nature* **1972**, *238* (5358), 37–38.
[13]. Toivola, M.; Halme, J.; Miettunen, K.; Aitola, K.; Lund, P. D. Nanostructured dye solar cells on flexible substrates-Review. *Int. J. Energy Res.* **2009**, *33* (13), 1145–1160.
[14]. Han, F.; Kambala, V. S.; Srinivasan, M.; Rajarathnam, D.; Naidu, R. Tailored titanium dioxide photocatalysts for the degradation of organic dyes in wastewater treatment: A review. *Appl. Catal. A: Gen.* **2009**, *359* (1-2), 25–40.
[15]. Kubiak, B.; Piszczek, P.; Radtke, A.; Muzioł, T.; Wrzeszcz, G.; Golińska, P. Photocatalytic and Antimicrobial Activity of Titanium(IV)-Oxo Clusters of Different Core Structure. *Crystals* **2023**, *13* (7), 998.
[16]. Hong, Z.; Xu, S.; Yan, Z.; Lu, D.; Kong, X.; Long, L.; Zheng, L. A Large Titanium Oxo Cluster Featuring a Well-Defined Structural Unit of Rutile. *Cryst. Growth amp; Des.* **2018**, *18* (9), 4864–4868.
[17]. Rozes, L.; Sanchez, C. Titanium oxo-clusters: precursors for a Lego-like construction of nanostructured hybrid materials. *Chem. Soc. Rev.* **2011**, *40* (2), 1006.
[18]. Tomita, K.; Petrykin, V.; Kobayashi, M.; Shiro, M.; Yoshimura, M.; Kakihana, M. A Water-Soluble Titanium Complex for the Selective Synthesis of Nanocrystalline Brookite, Rutile, and Anatase by a Hydrothermal Method. *Angew Chem Int Ed* **2006**, *45* (15), 2378–2381.
[19]. Coppens, P.; Chen, Y.; Trzop, E. Crystallography and Properties of Polyoxotitanate Nanoclusters. *Chem. Rev.* **2014**, *114* (19), 9645–9661.
[20]. Nunzi, F.; De Angelis, F. Modeling titanium dioxide nanostructures for photocatalysis and photovoltaics. *Chem. Sci.* **2022**, *13*, 9485–9497.
[21]. Nath, J. K. Syntheses and Crystal Structures of Dinuclear Metallacycles of Mn(II), Co(II), Ni(II), Cu(II) and Cd(II) of 1,8-Naphthalene

Dicarboxylate Exhibiting Dihydrogen Contact. *J. Struct Chem* **2023**, *64* (6), 1021–1039.
[22]. Nath, J. K. Syntheses, structural insight and hirshfeld surface analysis of two heteroleptic coordination polymer of Cu(II). *J. Struct Chem* **2023**, *64* (9), 1664–1676.
[23]. Nath, J. K.; Mondal, A.; Powell, A. K.; Baruah, J. B. Structures, Magnetic Properties, and Photoluminescence of Dicarboxylate Coordination Polymers of Mn, Co, Ni, Cu Having *N*-(4-Pyridylmethyl)-1,8-naphthalimide. *Cryst. Growth amp; Des.* **2014**, *14* (9), 4735–4748.
[24]. Nath, J. K.; Kirillov, A. M.; Baruah, J. B. Unusual solvent-mediated hydrolysis of dicarboxylate monoester ligands in copper(ii) complexes toward simultaneous crystallization of new dicarboxylate derivatives. *RSC Adv,* **2014**, *4* (88), 47876–47886.
[25]. Wang, Z.; Gupta, R. K.; Alkan, F.; Han, B.; Feng, L.; Huang, X.; Gao, Z.; Tung, C.; Sun, D. Dicarboxylic Acids Induced Tandem Transformation of Silver Nanocluster. *J. Am. Chem. Soc.* **2023**, *145* (36), 19523–19532.
[26]. Wang, C.; Liu, C.; Li, L. J.; Sun, Z. Synthesis, Crystal Structures, and Photochemical Properties of a Family of Heterometallic Titanium Oxo Clusters. *Inorg. Chem.* **2019**, *58* (9), 6312–6319.
[27]. Chebbi, S.; Allouche, A.; Schwarz, M.; Rabhi, S.; Belkacemi, H.; Merabet, D. Treatment of produced water by induced air flotation: effect of both TWEEN 80 and ethanol concentrations on the recovery of PAHs. *Nova Biotechnol. Chim.* **2018**, *17* (2), 181–192.
[28]. Irshad, R.; Asim, S.; Mansha, A.; Arooj, Y. Naphthalene and its Derivatives: Efficient Fluorescence Probes for Detecting and Imaging Purposes. *J. Fluoresc* **2023**, *33* (4), 1273–1303.
[29]. Bruker (2009). APEX2. Bruker AXS Inc., Madison, Wisconsin, USA.
[30]. Sheldrick, G. M. Crystal structure refinement with*SHELXL*. *Acta Crystallogr C. Struct Chem* **2015**, *71* (1), 3–8.
[31]. Dolomanov, O. V.; Bourhis, L. J.; Gildea, R. J.; Howard, J. A.; Puschmann, H. *OLEX2*: a complete structure solution, refinement and analysis program. *J. Appl Crystallogr* **2009**, *42* (2), 339–341.
[32]. Spek, A. L. Structure validation in chemical crystallography. *Acta Crystallogr D. Biol Crystallogr* **2009**, *65* (2), 148–155.
[33]. Macrae, C. F.; Sovago, I.; Cottrell, S. J.; Galek, P. T.; McCabe, P.; Pidcock, E.; Platings, M.; Shields, G. P.; Stevens, J. S.; Towler, M.; Wood, P. A. *Mercury 4.0*: from visualization to analysis, design and prediction. *J. Appl Crystallogr* **2020**, *53* (1), 226–235.
[34]. Brandenburg, K.; Putz, H. 1999, DIAMOND. Crystal Impact GbR, Bonn, Germany.
[35]. Radtke, A.; Piszczek, P.; Muzioł, T.; Wojtczak, A. The structural conversion of multinuclear titanium(IV) μ-oxo-complexes. *Inorg. Chem.* **2014**, *53*, 10803–10810.
[36]. Spackman, P. R.; Turner, M. J.; McKinnon, J. J.; Wolff, S. K.; Grimwood, D. J.; Jayatilaka, D.; Spackman, M. A. *CrystalExplorer*: a program for Hirshfeld surface analysis, visualization and quantitative analysis of molecular crystals. *J. Appl Crystallogr* **2021**, *54* (3), 1006–1011.
[37]. Tsering, D.; Dey, P.; Kapoor, K. K.; Seth, S. K. An Energetic and Topological Approach to Understanding the Interplay of Noncovalent Interactions in a Series of Crystalline Spiropyrrolizine Compounds. *ACS Omega* **2024**, *9*, 36242–36258. https://doi.org/10.1021/acsomega.4c02511.
[38]. Gumus, I.; Solmaz, U.; Binzet, G.; Keskin, E.; Arslan, B.; Arslan, H. Hirshfeld surface analyses and crystal structures of supramolecular self-assembly thiourea derivatives directed by non-covalent interactions. *J. Mol. Struct.* **2018**, *1157*, 78–88.
[39]. de Almeida, L. R.; Carvalho, P. S.; Napolitano, H. B.; Oliveira, S. S.; Camargo, A. J.; Figueredo, A. S.; de Aquino, G. L.; Carvalho-Silva, V. H. Contribution of Directional Dihydrogen Interactions in the Supramolecular Assembly of Single Crystals: Quantum Chemical and Structural Investigation of $C_{17}H_{17}N_3O_2$ Azine. *Cryst. Growth amp; Des.* **2017**, *17* (10), 5145–5153.
[40]. Prins, L. J.; Reinhoudt, D. N.; Timmerman, P. Noncovalent synthesis using hydrogen bonding. *Angew. Chem. Int. Ed Engl.* **2001**, *40*, 2382–2426.
[41]. Echeverría, J.; Aullón, G.; Danovich, D.; Shaik, S.; Alvarez, S. Dihydrogen contacts in alkanes are subtle but not faint. *Nature Chem* **2011**, *3* (4), 323–330.
[42]. Echeverría, J.; Aullón, G.; Alvarez, S. Dihydrogen intermolecular contacts in group 13 compounds: H···H or E···H (E = B, Al, Ga) interactions?. *Dalton Trans.* **2017**, *46* (9), 2844–2854.
[43]. Islam, S.; Dey, P.; Seth, S. K. Structural elucidation and various computational studies for quantitative investigation of intermolecular interactions in pyridine-2,6-dicarboxylic acid and its di-hydrate. *J. Mol. Struct.* **2024**, *1311*, 138433.
[44]. Znovjyak, K.; Seredyuk, M.; Malinkin, S. O.; Shova, S.; Soliev, L. Crystal structure of {N^1,N^3-bis[(1-benzyl-1*H*-1,2,3-triazol-4-yl)methylidene]-2,2-dimethylpropane-1,3-diamine}bis(thiocyanato-κ*N*)iron(II). *Acta Crystallogr E. Cryst Commun* **2020**, *76* (10), 1661–1664.
[45]. Chaisuriya, W.; Chainok, K.; Wannarit, N. Crystal structure and Hirshfeld surface analysis of a new mononuclear copper(II) complex: [bis-(pyridin-2-yl-κN)amine](formato-κO)(m-hy-droxy-benzoato-κ2O,O')copper(II). *Acta Crystallogr. E Crystallogr. Commun.* **2023**, *79*, 1115–1120.
[46]. Al-Dies, A. M.; Alblewi, F. F.; Okasha, R. M.; Alsehli, M. H.; Borik, R. M.; Ihmaid, S.; Amr, A. E.; Ghabbour, H. A.; Elhenawy, A. A.; El-Agrody, A. M. Synthesis, crystal structure, hirshfeld study, DFT analysis, molecular docking study, antimicrobial activity of β-enaminonitrile bearing 1H-pyran. *Discov Appl Sci* **2025**, *7* (1), https://doi.org/10.1007/s42452–024–06254–w.
[47]. Qin, Z.; He, J.; Zhu, Y.; Wei, X.; Wang, J.; Zheng, G.; Mo, S.; Zhou, B.; Long, F. Crystal structure and electrical conduction of the new organic-inorganic compound (C7H10N)2MnCl4. *J. Mol. Struct.* **2023**, *1281*, 135080.
[48]. Abdullah, S.; Deka, S.; Abid, F.; Sharma, S.; Nath, J. K.; Rajbongshi, B. K. Synthesis, structural investigation and Hirshfeld surface analyses of two imidazolinone based heterocyclic compounds. *J. Struct. Chem.* **2024**, *65*, 1805–1815.
[49]. Nath, J. K.; Borah, R. A lanthanide cluster formed by fixing atmospheric CO2 to carbonate: a molecular magnetic refrigerant and photoluminescent material. *J. Chem Sci* **2023**, *135* (3), https://doi.org/10.1007/s12039–023–02176–z.
[50]. Nath, J. K. Synthesis, supramolecular insight, Hirshfeld surface analyses and optical properties of Fe(II) and Cu(II) complexes of flexible imidazole tethered 1,8-naphthalimide. *Transit Met Chem* **2024**, *49* (3), 171–181.
[51]. Stenfors, B. A.; Ngassa, F. N. Crystal structure of 2,4-dinitrophenyl 2,4,6-trimethylbenzenesulfonate. *Eur. J. Chem.* **2022**, *13* (2), 145–150.